Digest of Translated Russian Literature

The following abstracts have been selected by the Editor from translated Russian journals supplied by the indicated societies and organizations, whose cooperation is gratefully acknowledged. Information concerning subscriptions to the publications may be obtained from these societies and organizations. Note: Volumes and numbers given are those of the English translations, not of the original Russian.

INSTRUMENTS AND EXPERIMENTAL TECHNIQUES (Pribory i Tekhnika Eksperimenta). Published by Instrument Society of America, Pittsburgh, Pa.

Number 1, September 1961

High Frequency Ion Source with Discharge in Salt Vapors, V. F. Kozlov, V. L. Marchenko, and Ya. M. Fogel', pp. 21–24.

We describe the design of a high frequency ion source with discharge in salt vapors, as well as the results obtained in investigating the characteristics of this source. Ion currents of ~1 ma were obtained. Under optimum operating conditions, the ion beam contains up to 90% of atomic metal ions. The average lifetime of the source is 50 hr. The average material consumption is 30 mg/hr.

High frequency ion sources with discharge in hydrogen are widely used in accelerator techniques for the production of hydrogen ion beams. Investigations of such sources have been well-described in surveys. Ion beams of inert gases, nitrogen, carbon and oxygen, chlorine, and boron and fluorine were also obtained by means of high frequency ion sources. Gaseous compounds of the elements whose ions were to be obtained were used for producing these ions. Thus, for producing C^+, Cl^+, B^+, and F^+ ions, the CO_2, CCl_2, F_2, and BF_3 gases were used.

However, the production of beams of certain ions, in particular, metal ions, is difficult because the elements corresponding to these ions do not form gaseous compounds. These difficulties can be overcome by creating ion beams from the discharge plasma in vapors of hard compounds of elements whose ions are to be obtained. This method is widely used in ion sources for electromagnetic separators. In these sources, the ion beam is extracted from arc discharge in a magnetic field. For the production of ion beams of great intensity with currents of the order of several tens or hundreds of milliamperes, use of such sources is entirely justified regardless of their short lifetime (rapid disintegration of the hot cathode), large feed power, and large dimensions. Where ion beams with a current of ~1 ma are required, it is desirable to have a small source with a relatively low feed power. This problem has been solved here by designing a high frequency ion source with discharge in vapors of hard compounds of some metals. The design of this source, the method of its utilization, and some of its characteristics are described.

Ion Source with Surface Ionization for the Separation of Isotopes of Alkali Elements, V. I. Raiko, M. S. Ioffe, and V. S. Zolotarev, pp. 25–27.

The design of an ion source with surface ionization for the production of intensive K and Rb ion beams in electromagnetic separating devices is described. In comparison with gas discharge sources, this source has certain advantages resulting from the absence of gas discharge: the effect of the oscillatory process arising in discharge on the ion beam is eliminated, the ion spectrum does not contain ions with multiple charges, etc. The source operating characteristics and the results obtained in separating K and Rb isotopes are given.

The source of an electromagnetic separating device must satisfy the following basic requirements—it must produce a well-focused ion beam with a maximum possible current intensity, have a high value of the working material utilization factor, and be capable of stable and continuous operation over a long period of time.

Ion sources with ionization of the vapors of the element to be separated by electronic impact in gas discharge are ordinarily used. The main advantage of this ionization method is that it provides the possibility of producing ions of any element or compound. However, in the ionization of atoms and molecules by electronic impact, we obtain the complete spectrum of ions with different e_0/m ratios; these ions cannot be used simultaneously in the separation process. Another disadvantage is the dependence of the position and shape of the "emitting" plasma surface on the discharge parameters. Moreover, the oscillatory processes arising in arc discharge can result in the decompensation of the ion beam space charge, which reduces the output of such ion sources. For the separation of isotopes of certain alkali elements, we can use a different ionization method, namely, the surface ionization method, which is free from the foregoing drawbacks. As is well known, the surface ionization effect is successfully used for the production of alkali, alkaline earth, and rare earth element ions in mass spectrometry. However, so far as we know, sources of this type have not been used in electromagnetic separating devices. The present article describes an ion source with surface ionization, which is designed for the separation of K and Rb isotopes in large quantities.

Determination of Particle Charge Sign in Photoemulsions, I. M. Gramenitskii, Z. Korbel, and L. Rob, pp. 39–41.

The magnetic deflection of charged secondary particles was measured in an emulsion stack which was irradiated by an internal beam of protons with an energy of ~9 Bev and which was located in the magnetic field of a synchrophasotron (field strength: ~1.2 koe) during irradiation. The possibility of the statistical separation of particles with respect to the charge sign for track lengths $t \sim 6$–10 cm was demonstrated.

Determination of the Natural Amplitude Resolution of Photomultipliers by Means of a Pulsed Light Source, V. V. Matveev and A. D. Sokolov, pp. 74–77.

We discuss certain problems of the methodology used in determining the natural half-width of the amplitude distribution of light flashes from pulsed light sources and in determining the resolving power of photomultipliers. We describe a pulsed light source with a TKh-4B thyratron with a natural half-width of the light pulse amplitude distribution of not more than 1% and an amplitude stability not worse than 2.5% for a period of 8 hr of continuous operation.

Limiter Whose Limiting Threshold Is Proportional to the Acting Pulse Amplitude, I. M. Kuks, p. 99.

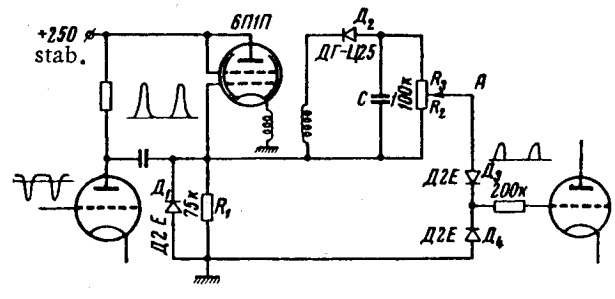

Fig. 1

In designing photoelectronic devices for ionization measurements in nuclear emulsions, it is sometimes necessary to transform a series of pulses with flat fronts into a series of pulses whose duration is equal to the half width of the initial pulses. The main difficulty encountered here is that the amplitude of the initial pulses can change slowly within a single series (measurement of discontinuities) or in different series (width measurements). The

voltage level corresponding to the half width will be determined by the pulse amplitude and, where a conductive coupling is used in the preceding circuit, also by the pulse duty ratio. This problem can be solved by the circuit proposed in Fig. 1.

Sensitive Current Integrator, V. Ya. Golovnya, I. I. Zalyubovskii, and V. A. Shilyaev, pp. 100–101.

Sensitive Magnetometer with a Compensating Coil, V. H. Lukashev, pp. 153–156.

The author describes the principle of operation, design, and parameters of a sensitive magnetometer with a compensating coil that is capable of measuring a magnetic field of 20 oe and greater with an accuracy of 0.01%.

Laboratory Precision Cryostat for Investigating Electrical and Elastic Properties of Crystals, V. A. Koptsik, B. A. Strukov, and L. A. Ermakova, pp. 190–194.

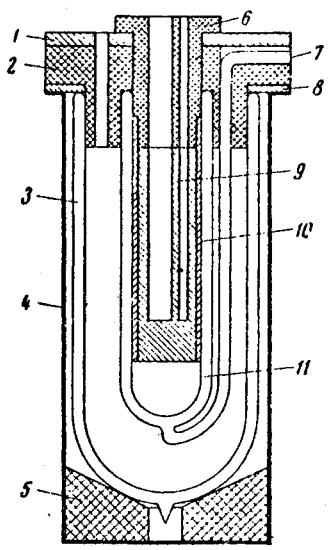

Fig. 1. Cryostat design. 1) Textolite lid; 2) covering made of porous PS-4 plastic; 3) outside Dewar flask; 4) protective tin plate casing; 5) wooden support block; 6) ebonite plug; 7) glass branch pipe for connection to pump; 8) rubber gasket; 9) copper block; 10) aluminum screen; 11) internal glass vessel.

A low temperature thermostat which operates in the room temperature to −140°C interval is described. An arrangement has been provided for securing stabilized temperature points; the thermostatic control accuracy is not worse than ±0.005°C over a period of 1 hr, and it is sufficient for precision dielectric measurements.

Metallic Cryostat for Optical Investigations of Solids at Low Temperatures, E. N. Lotkova and A. B. Fradkov, pp. 194–195.

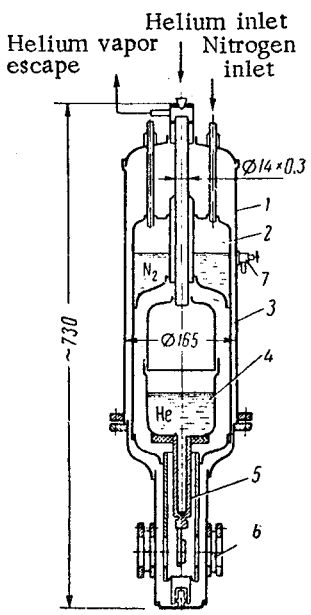

Cryostat for optical investigations. 1) Frame; 2) nitrogen bath container; 3) screen; 4) helium bath; 5) cold conductor; 6) window for specimen illumination; 7) evacuation valve.

High Pressure Chamber for Optical Investigations at Low Temperatures, A. K. Tomashchik, pp. 200–201.

Investigations of the effect of hydrostatic compression on the optical and photoelectric properties of crystals at low tempera-

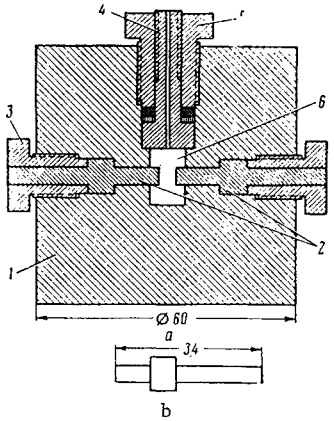

Fig. 1. High-pressure chamber. 1) Frame; 2) windows; 3) shutter; 4) mushroom-shaped element; 5) nut of the mushroom-shaped element; 6) working volume; b) methylmethacrylate window.

tures are of great scientific and, in certain cases, practical interest. However, lack of substances which would be transparent and at the same time able to transmit pressure at low temperatures makes these investigations difficult. The present paper is concerned with the design of a high pressure chamber for optical and photoelectric investigations at low temperatures.

Introduction of Fixed Amounts of Mercury into Vacuum Systems, L. Paty and L. Plihta, pp. 204–205.

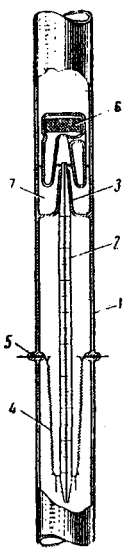

Device for introducing mercury into a vacuum system. 1) Glass cylinder; 2) capillary with scale; 3) ground section; 4) tungsten spirals; 5) molybdenum lead-ins; 6) float with iron core; 7) mercury.

Fixed amounts of high purity mercury must be introduced into some vacuum systems. The corresponding methods described in the literature are inaccurate, and they cannot be used for dosing amounts of mercury weighing less than 0.1 g. If mercury is introduced by means of a modified dosing cock valve and, especially, if the manual method, where separate doses are weighed, is used, the necessary degree of mercury purity cannot be secured. A device which makes it possible to introduce high purity mercury into vacuum systems in doses weighing not less than 1.5 mg with an accuracy of $5 \cdot 10^{-2}$ mg has been developed.

Number 2, December 1961

Injector of Negative Hydrogen Ions, Yu. M. Khirnyi and L. N. Kochemasova, pp. 226–230.

An account is given of the design and experimental study of the focusing system of two versions of a negative hydrogen ion injector for a 2 × 1.5 Mev charge-exchange electrostatic generator.

Summary:

1) The chosen electron-optical focusing system produces H_1^- currents with the required beam parameters (diameter and angular divergence). In the entire working energy range, the diameter of the main part of the beam in the object plane is D = 2–3 mm, and the maximum divergence angle is θ = 0.016 rad, which is less than the maximum allowed by the tube focusing conditions (0.1 rad).

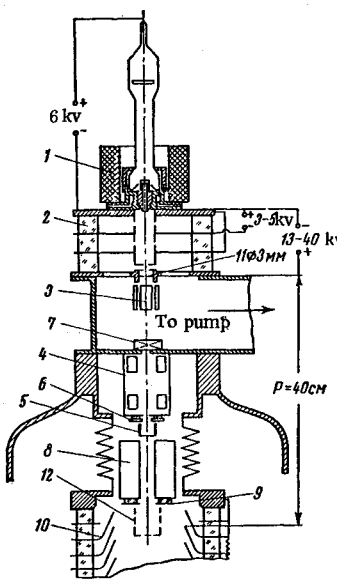

Fig. 3. Schematic of H_1^- injector: 1) source of H_1^- ions; 2) focusing device; 3) corrector; 4) electron separator; 5) Faraday cylinder L-1; 6 and 9) electrodes for suppressing secondary electrons; 7) valve; 8) trap; 10) tube; 11) diaphragm; 12) Faraday cylinder L-2.

2) When the source is operated in conjunction with the magnetic analyzer, there is no change in the focusing of the beam.

3) Insertion of the diaphragm in the lower electrode of the immersion lens cuts down the current of fast H_1^0 particles injected into the tube very considerably, and, most important, lets them through with a very small angular divergence, which prevents them from reaching the tube electrodes. The ground-to-ground electrostatic generator can then be operated without an analyzer at the output of the source.

4) The foregoing system of injection of H_1^- ions into the tube of the Alvarez electrostatic generator, which incorporates rigid stabilization of the narrowest part of the beam in the object plane of the tube with the aid of a diaphragm, is much simpler than that described by Gollins and Riviere. It consists of two lenses instead of four and has much smaller dimensions (the length of the focusing system of the injector up to the object plane of the tube is 120 and 170 mm instead of 4250 mm). The beam obtained in the object plane has a smaller diameter, which is practically independent of the input energy.

Measurement of Ionization in Type-R Emulsions, A. O. Vaisenberg, E. D. Kolganova, N. V. Rabin, and E. A. Pesotskaya, pp. 266–269.

The possibility of measuring the density effect in type-R emulsions is investigated. The magnitude of the maximum relativistic increase is 13%. One of the methods of determining ionization in nuclear emulsions is to count the number of gaps or to measure the average length of gaps between aggregates of developed AgBr crystals forming the track of a charged particle.

It was shown elsewhere that in the ionization range $i_{\min} \leq i \leq 5000$ grains/mm, the integral distribution of the gap lengths is of the form

$$ne = n_0 \exp(-gl) \qquad [1]$$

where l is the gap length in microns, n_e the number of gaps $\geq l$ per mm, and n_0 the total number of gaps per mm, i.e., the blob density.

The distribution parameter g represents the reciprocal of the average gap length, or the true number of grains per unit length. Within the limits of this range of ionizations, the parameter is proportional to the ionization loss. The ionization due to a charged particle is usually characterized by the quantity $g^* = g/g_0$ where g_0 is the value of g for singly charged relativistic particles ($\gamma = E/mc^2 \gg 1$). It must be noted that g^* is but little dependent on the magnitude of the relativistic ionization, the degree of development, or the personal equation of the observer. The parameter g^* is, therefore, very convenient for describing the ionization.

Study of the Dependence of Distortions and Spurious Scattering on the Dip Angle of Tracks in Nuclear Emulsions, Wang Shu-fen, N. Dalkhazhav, R. M. Lebedev, V. N. Strel'tsov, pp. 269–271.

Dependence of distortions and spurious scattering on the dip angle of a charged particle track in NIKFI-R emulsions has been investigated. Measurements were carried out on tracks with dip angles of 0.5, 1.2, 2.1, 2.9, 5.6, and 10. It was established that distortions become appreciable for dip angles greater than 3° and are largely of C-shaped character. Spurious scattering was found to be independent of the dip angle within the range 0–10°. Relations have been obtained between 2nd, 3rd, and 4th coordinate differences for spurious scattering.

Transistorized Amplifier for Spectrometry, L. S. Gorn, L. S. Zhurina, and B. I. Khazanov, pp. 298–299.

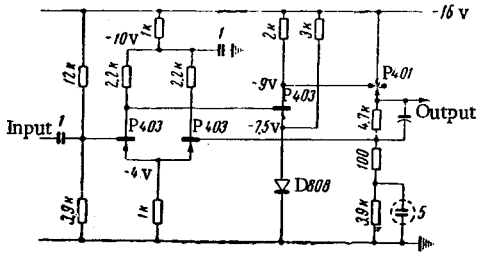

Fig. 1. Circuit of a three-stage amplifier with resistance coupling.

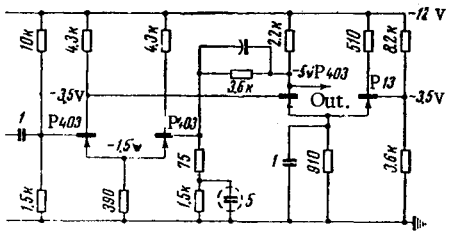

Fig. 2. Circuit of an amplifier using differential stages with resistance coupling.

Amplifier circuits with semiconductor triodes for the amplification of pulses from scintillation pickups, which differ from previously described devices by resistive interstage coupling, can be of practical interest. Two versions of this circuit are shown in Figs. 1 and 2; Fig. 1 shows an amplifier that is based on a circuit 'of three," whereas Fig. 2 shows an amplifier based on a circuit "of two."

Photoelectric Method of Extracting Weak Pulse Signals, V. I. Chernysh, pp. 306–309.

A description is given of a photoelectric selection device for recovering weak echo signals from almost motionless meteorological objects. The improvement in the signal-to-noise ratio relative to an ordinary radar system is 16 db for an averaging time of 3 sec.

Transistorized Input Amplifier for a Bolometer, M. N. Markov, pp. 325–326.

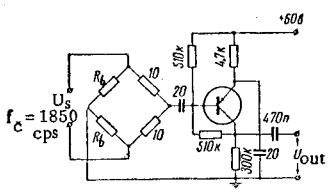

Fig. 1. Input circuit of a bolometer amplifier with a transistor.

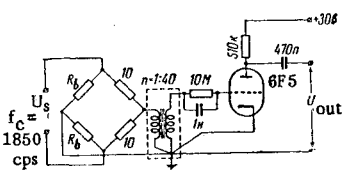

Fig. 2. Input circuit of a bolometer amplifier with an input transformer.

The following Russian abbreviations are retained in the figure: л = tube, Тр = transformer, М = megohm, к = kilohm, мк = μf or μh, н = mμf or mμh, п = μμf or μμh, and в = volt. For individual tube designations see appendix to No. 1 of this year.

Device for Investigation of Creep in Metals and Recording of Its Origin, A. A. Predvoditelev, pp. 372–374.

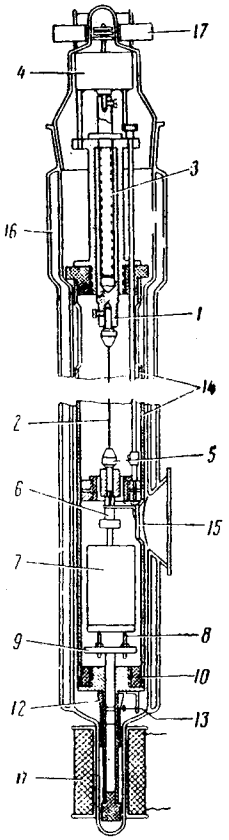

Fig. 1. Design of the device for the investigation of creep in fine metal wires.

Creep is a slow change in the dimensions of a body due to the application of a constant load. Since creep is in effect a direct continuation of an instantaneous deformation, the determination of the moment when the loading process ends and creep begins presents some difficulties. The initial part of the process of creep is characterized by a considerable rate of strain; therefore, even a very small error in determining its beginning can introduce a substantial error into the value of the general strain.

By the device shown in Fig. 1 this error can be essentially eliminated and a creep curve obtained which begins at the moment when the maximum load has been reached. The upper part of the device carries the grip 1 which holds one of the ends of the fine wire specimen 2. The grip 1 can be moved by means of the screw 3, which is driven by an SD-2 fractional-horsepower motor

Fast-Acting Electrical Hydraulic Shock Valve for Wilson Cloud Chambers, V. F. Vishnevskii and V. V. Ekaterinin, pp. 378–379.

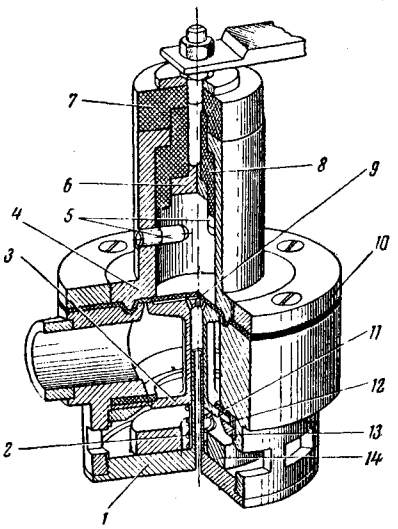

Assembled electrical hydraulic shock valve. 1) Housing lid with guiding stem; 2) spring; 3) the valve proper; 4) discharge head frame; 5) electrodes; 6) high-voltage lead-in; 7) insulators; 8) insulating rubber gasket; 9) diaphragm; 10) tightening ring; 11) rubber gasket; 12) washer; 13) nut; 14) foam rubber cushion.

4. The lower part of the device has the grip 5 which holds the opposite end of the specimen 2. The grip 5 also carries the suspension member 6 with the weight 7. This weight rests on three points 8 of the support 9. The adjustable points 8 are arranged in such a manner that the axis of the suspension member 6 with weight 7 is vertical. The support 9 is electrically isolated from the body of the device by a hard rubber ring 10. The lower part of the device also includes the electromagnetic relay 11, adjustable iron core 12 with tapered end, and the locking device 13. The pipe 14, which has holes to facilitate assembly, joins the top and bottom parts of the device to form a single unit. For measuring the creep strain the central part of the device carries the mirror 15 which, during the elongation of the specimen, rotates about the horizontal axis. For maintaining the temperature constant the whole device is placed into a double-walled glass cylinder 16. The stator 17 of the motor is arranged on the outside of the glass cylinder's lid.

Liquid Helium Level Indicator, A. E. Rovinskii, p. 398.

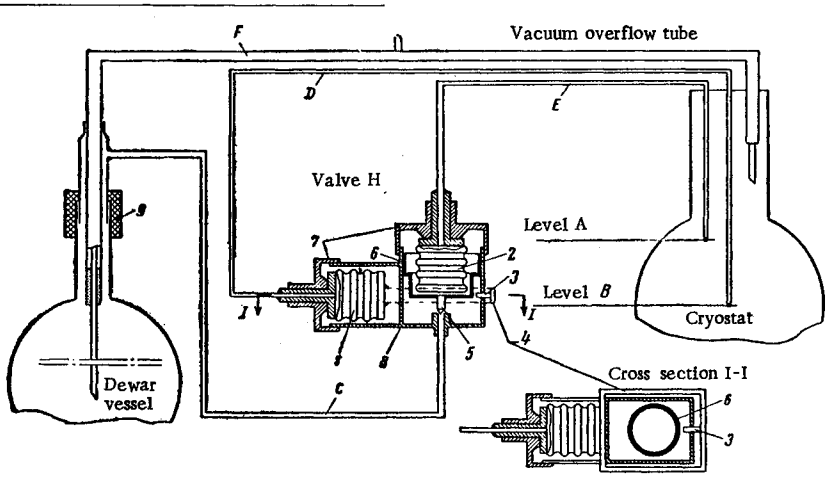

1 and 2) Bellows; 3) latch; 4) connection; 5) valve; 6) sleeve; 7) lid; 8) body; 9) rubber sleeve; C) tube; D and E) tubes filled with oxygen; F) overflow.

Graphical Method of Calculating Particle Energies in a Moving Coordinate System from Their Values in the Laboratory Coordinate System, Yu. I. Serebrennikov, pp. 380–381.

High Frequency Mechanical Light Chopper, A. A. Meier, pp. 391–392.

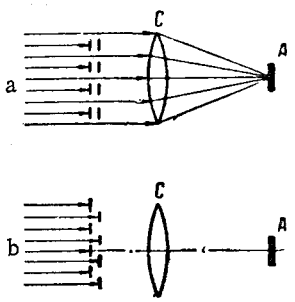

Fig. 1

A chopper of the proposed design can provide high modulation frequency combined with high light intensity. The principle of operation of the chopper is clear from Fig. 1. A parallel beam of light passes through two gratings moving in opposite directions and is focused by lens C on the object A. It is obvious that the light intensity on the surface of object A will be greatest when the gratings are in the position shown in Fig. 1a. When the gratings are in the position shown in Fig. 1b, the light beam will be cut off. Since a parallel bunch of rays passes through the gratings, the latter act as a diaphragm and do not affect the uniformity of illumination of the object. If the grating constant is d and the relative velocity of the gratings is v, the modulation frequency is

$$\nu = v/d$$

For full modulation, the width of the slits must not exceed $d/2$.

Number 6, July 1962

Homogeneous Crystal Counters, B. M. Golovin, B. P. Osipenko, and A.I. Sidorov, pp. 1045–1052.

An account is given of the history of research, basic properties, and some applications of homogeneous crystal counters constructed from various materials.

The investigations of radiation-induced conductivity in dielectrics can probably be considered the initial experiments which led ultimately to construction of crystal counters for registration of single charged particles. The level of experimental technique at that time did not permit the observation of conduction pulses caused by single particles, and only the integral conduction due to the effect of a large number of particles (or quanta) was investigated. These devices were the direct predecessors of the crystal dosimeters of later date.

The first description of a crystal counter capable of registering single nuclear particles can be found in another paper, where silver chloride crystals at liquid nitrogen temperature were used. Shortly after, an integral increase in conductivity of cadmium sulfide single crystals at room temperature under the action of γ and β rays was observed, and the possibility of employing these crystals in appropriate conditions as crystal counters was noted. The registration of single particles by cadmium sulfide single crystals was described elsewhere. The first observations of conduction pulses in diamond when single charged particles fell on it were probably those made in another study.

The results of previously described experiments on the use of halides at low temperatures as crystal counters were further developed in other studies.

One of the principal faults of most dielectric counters is the diminution in pulse height during the count, owing to electric polarization of the crystal. Many studies have been devoted to methods of eliminating this fault.

Phase Stability in Amplifiers with Arbitrary High Frequency Field Configurations, A. N. Lebedev, pp. 1059–1062.

A general phase equation for cyclic accelerators with arbitrary high frequency field configurations and equilibrium orbits is derived. In general form, it is shown that the law governing the dampening of synchrotron oscillations cannot be changed by modifying the accelerating system; this law is completely defined by the dependence of the loss magnitude on the particle energy.

In the first papers on automatic phase control in cyclic accelerators, it was found that synchrotron oscillations are not characterized by self-dampening in the absence of radiation. However, assumptions about the high frequency (hf) field configuration that were used did not make it possible to generalize this result, although it remained valid for all of the fairly diversified accelerating systems of operative accelerators. Despite this, several proposals concerning this problem have been advanced, since the possibility of securing the damping of synchrotron oscillations by modifying the accelerating system is very attractive. For instance, it was stated in various papers that dampening can be caused by the finite dimensions of the accelerating slit, by bending the slit, by the dependence of the hf voltage amplitude on the radius, etc. More detailed analysis of each of these proposals showed that they were erroneous.

Interest in this problem has revived recently, since the possibility of artificial dampening of synchrotron oscillations would be extremely valuable for high energy electron accelerators as well as for accumulating systems. It is of interest to consider this problem in its most general form without restriction to any special orbit and hf field configuration.

Diffusion Cloud Chamber Controlled by a Photoelectric Multiplier, V. K. Lyapidevsky and M. M. Obodovsky, pp. 1078–1081.

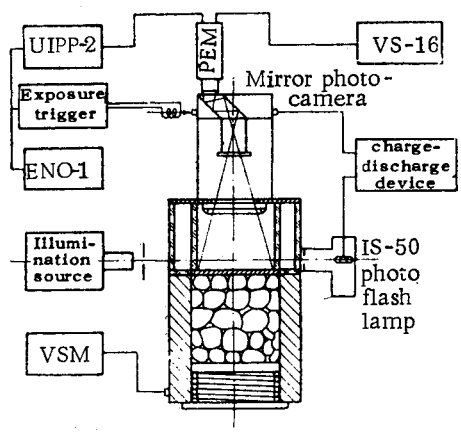

Fig. 1. Schematic drawing of cloud chamber and block diagram of apparatus.

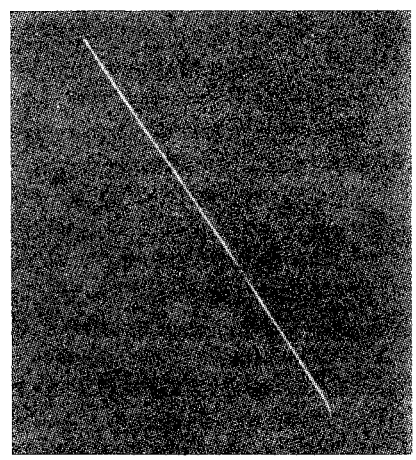

Fig. 2 Photograph of α-particle track

A diffusion cloud chamber is described which is controlled by a photoelectric multiplier. Photographs of α-particle tracks which were obtained by means of this apparatus are presented, along with photographs of the initial stages of the discharge taking place in the chamber atmosphere. The dependence of the magnitude of the droplet background and its fluctuations on the diffusing vapor flow and the ion load is investigated. It is shown that with changes of the vapor flow over a wide range the supersaturation in the sensitive layer remains substantially unchanged.

Gaseous Discharge Chamber, A. M. Govorov, V. I. Nikanorov, G. Peter, A. F. Pisarev, and Kh. Poze, pp. 1089–1091.

Operational characteristics of a gaseous discharge chamber are given using electrodes spaced 70 mm apart.

One of the promising methods for recording charged particles uses a gaseous discharge chamber as a tracking element which was proposed in other papers. These chambers differ from the ordinary spark gap chambers in that their electrodes are separated from the working space by a dielectric material. Investigations have shown that with an electrodes separation of 20 mm, the width of the tracks obtained is 2 mm, the average angle of inclination of the discharge path along the trajectory of the particle with respect to the electric field direction is 18°, and the duration of sensitivity equals 6 to 10μsec. In the present article, similar characteristics of chambers with larger interelectrode gaps are investigated. Furthermore, the problems of dependence of the high voltage pulse amplitude applied to the chamber on the pulse duration (provided a visible track is to be obtained) and the part played by the cleanup field, which have not been investigated elsewhere, are studied.

Ultra-High-Speed Pulse Oscillograph, L. S. Bartenev, G. V. Glebovich, and K. N. Ptitsin, pp. 1120–1122.

An oscillograph is described, with maximum spot velocity $2 \cdot 10^{10}$ cm/sec at a time instability not greater than $1.5 \cdot 10^{-11}$ sec, permitting pulse processes of duration 10^{-10} sec to be registered.

Device for Calibrating Sensitivities of Ion Current Measurement Channels of Dual-Beam Mass Spectrometers, I. V. Gol'denfel'd and I. Z. Korostyshevskii, pp. 1122–1125.

A method and a device for calibrating the sensitivity ratio of the measuring channels of dual-beam mass spectrometers without performing isotopic analysis are described. The calibration accuracy is not worse than $\pm 0.02\%$. This method can also be used for determining the absolute values of high resistance resistors and for checking their linearity.

New Photomultipliers, G. S. Vil'dgrube, N. V. Dunaevskaya, and I. A. Kharitonova, pp. 1130–1132.

The design of photomultipliers FEU-52 and FEU-53 is described, and their parameters, characteristics, and recommended operating conditions are presented.

Table 1

Characteristics and parameters	FEU-53	FEU-52
Overall length, mm	117.0	125.0
Envelope diameter, mm	51.3	80.0
Photocathode diameter, mm	45.0	75.0
Number of multiplier stages	14	12
Region of spectral sensitivity A	2500–6500	3000–8000
Spectromaximum A	4100 ± 100	4200 ± 100
Maximum quantum efficiency of photocathode, %	18.0	25.0
Integral sensitivity of photocathode, μamp/lu	40.0	80.0
Integral sensitivity at multiplier output, amp/lu	U_0=1700v 40	U_0=1700v 8
	U_0 = 2200v 4000	U_0=2200v 800
Dark current, amp	U_0=1700v $4 \cdot 10^{-7}$	U_0=1700v $5 \cdot 10^{-8}$
	U_0=2200v $2 \cdot 10^{-5}$	U_0=2200v $2 \cdot 10^{-5}$
Maximum output current, ma	10.0	10.0
Maximum supply voltage, kv	2.5	3.0
Amplitude resolution for Cs^{131} from NaI(Tl) crystal, %	9–11	9–12
Limit of light characteristic linearity with pulse illumination, amp	1.0	1.0
Current stability at output with V_0–1700 v, %	±2.5	±2.0
Noise equivalent energy in scale of NaI(Tl), kev	5.0	5.0
Pulse rise time at multiplier output, sec	$(4–5) \cdot 10^{-9}$	$(5–6) \cdot 10^{-9}$

Stabilizer of Photoluminescence Light Flux, N. I. Kuznetsov, pp. 1175–1176.

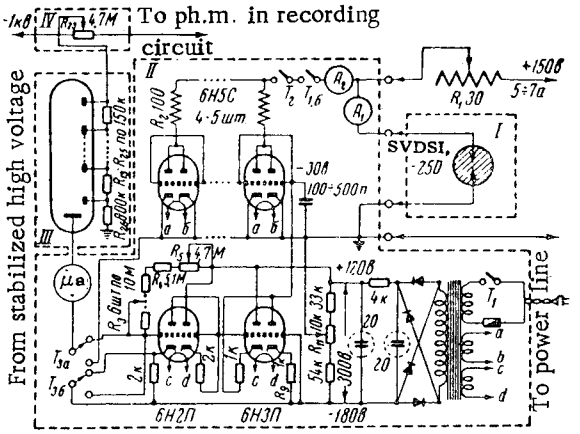

Circuit diagram of stabilizer: I) Excitation light source; II) stabilizer block; III) controlling photomultiplier; IV) distribution box for high voltages supplied to two ph.(oto) m(ultipliers).

An instrument is described which makes it possible dependably to stabilize photoluminescence flux by automatic adjustment of the excitation source potential. A photomultiplier exposed to the photoluminescence to be stabilized is used as the directing element of the control action. Only an insignificant part of the stabilized flux is used in this control action.

MEASUREMENT TECHNIQUES (Izmeritel'naia Tekhnika). Published by Instrument Society of America, Pittsburgh, Pa.

Number 1, September 1961

Uniformity of Measurements in the Sphere of Accelerometry, P. N. Agaletskii and V. I. Kiparenko, pp. 23–26.

Induction Transducer for Measuring Rapidly Changing Pressures, S. M. Gugel', pp. 27–28.

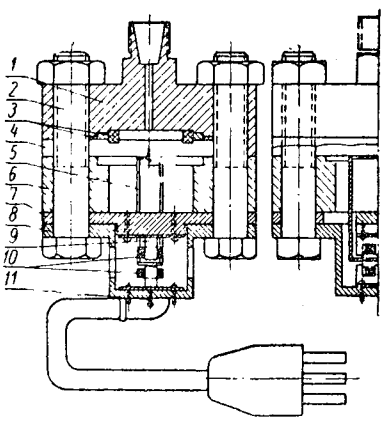

Fig. 1. Schematic of a high-pressure induction transducer. 1) Fuel receiver; 2) bolt with a nut; 3) packing; 4) diaphragm; 5) magnet coil; 6) thrust collar; 7) magnet holder; 8) lid; 9) core; 10) coil; 11) adjusting screw.

For investigating the value and nature of pressure variations in a fuel supply system for internal combustion engines we constructed a high-pressure induction transducer. Induction transducers have not been used previously for measuring high, rapidly changing pressures and, therefore, the satisfactory results we obtained in this respect are of some interest.

The main components of the transducer (Fig. 1) consists of two E-shaped cores 9 made of transformer iron. The cores carry